Development of polyamine substituted triphenylamine ligands with high affinity and selectivity for G-quadruplex DNA

Isabel Pont,[a, b] Álvaro Martínez-Camarena,[a] Cristina Galiana-Roselló,[a]Roberto Tejero,[c] M. Teresa Albelda,[a] Jorge González-García,[a, b] Ramón Vilar,[b] Enrique García-España[a]

Abstract: Currently significant efforts are devoted to designing small molecules able to bind selectively to guanine-quadruplexes (G4s). These non-canonical DNA structures are implicated in various important biological processes and have been identified as potential targets for drug development. Previously, we reported a series of triphenylamine(TPA)-based compounds including macrocyclic polyamines, which display high affinity towards G4 DNA. Following from this initial work, herein we present a series of second-generation compounds, in which the central TPA has been functionalised with flexible and adaptive linear polyamines, aiming to maximise the selectivity towards G4 DNA. The acid-base properties of the new derivatives have been studied by means of potentiometric titrations, UV-Vis and fluorescence emission spectroscopies. The interaction with G4s and duplex DNA has been explored using FRET melting assays, fluorescence spectroscopy and circular dichroism. Compared to our previously TPA derivatives with macrocyclic substituents, the new ligands reported herein retain the G4 affinity, but display two orders of magnitude higher selectivity for G4 *vs.* duplex DNA, most likely due to the ability of the linear substituents to embrace the G4 structure.

Introduction

There is an important need to identify new biomolecular targets for drug development. Examples of these less-studied targets in drug development are epigenetic proteins, membrane transporters, riboswitches and non-canonical nucleic acids.[1] Among non-canonical DNA structures, recently guanine (G)-quadruplexes (G4s) have gained significant interest as potential drug targets in cancer and neurological diseases. [2] G4s are oligonucleotide structures formed by the stacking of guanine quartets, which are planar supramolecular arrangements of four guanines held together by a hydrogen bonding network and electrostatic interactions with alkali metal ions (mainly potassium and sodium). [3]

A large number of putative G4-forming sequences has been identified in telomeres and promoter regions of various oncogenes [4] such as *c-Myc*, *kit*, *Ras* and *Bcl* and thus, G4s have been suggested to control proliferative activity during cancer. [5] In addition, expansions of G-rich sequences in the human genome, which lead to G4 formation, have been associated with neurological diseases, such as amyotrophic lateral sclerosis (ALS) or ataxia. [6] As a result, G-quadruplex structures have been proposed as potential targets for therapeutic intervention using small synthetic molecules. [2]

G4 DNA binders not only should have high affinity to the target, but also, they should display remarkable selectivity over duplex DNA, since this latter structure prevails among the genomic material. Significant efforts in the field have been dedicated to address this very challenging issue with some success. [7] As part of this effort, different polyamine-based compounds, both linear and macrocyclic, have demonstrated to be potential G4 DNA binders, even inducing the formation of this non-canonical structure from single-stranded DNA.[8] G4 binders usually contain a central aromatic core in order to enable the establishment of π-stacking interactions on the top of the G4 guanine-tetrads. In this context, the triphenylamine (TPA) moiety has been previously used for this aim, although solely in few studies.[9] Indeed, molecules containing TPA moieties have been mainly identified as minor groove binders in double-stranded DNA and used as photosensitizers in photodynamic therapy.[10] The combination of both molecular features in G4-binders (polyamines and TPA) has been firstly described by us, showing noteworthy affinity for G-quadruplex with moderate selectivity over double stranded DNA.[11]

Aiming to optimise the G4 over duplex DNA selectivity, we have prepared a series of second-generation of ligands in which the azacyclophane substituents have been replaced by linear polyamines. The conjunction of linear polyamines with the TPA scaffold enables to investigate the capability of the adaptive pending arms to embrace the G4 structure, while maintaining the TPA core stacked onto the top G-tetrad

Therefore, herein we present six novel compounds which include the TPA moiety as a central core and two different linear polyamines, *N,N*-dimethylethylenediamine and *N,N*-dimethyldipropylenetriamine, to analyse the effect of the molecular design on the interaction with different DNA structures.

[a] Dr. I. Pont, A. Martínez-Camarena, Dr. C. Galiana-Rosselló, Dra. M. T. Albelda, Dr. J. González-García and Prof. E. García-España
Department of Inorganic Chemistry, Institute of Molecular Science
University of Valencia
Catedrático José Beltrán 2, 46980 Paterna (Spain)
E-mail: enrique.garcia-es@uv.es

[b] Dr. I. Pont, Dr. J. González-García and and Prof. R. Vilar
Department of Chemistry
Imperial College London
White City Campus
London W12 OBZ
E-mail: r.vilar@imperial.ac.uk

[c] Prof. Roberto Tejero
Department of Physical Chemistry, University of Valencia
Dr. Moliner s/n, 46100 Burjassot (Spain)
E-mail: roberto.tejero@uv.es

The affinity and selectivity of the ligands for G-quadruplex DNA were assessed using emission spectroscopy, molecular modelling, FRET melting assays and CD spectroscopy. For these studies, we used a panel of G-quadruplex DNAs, which included different G4s topologies (hybrid, parallel and antiparallel), as well as double-stranded DNA displaying the most common B-type helix conformation.

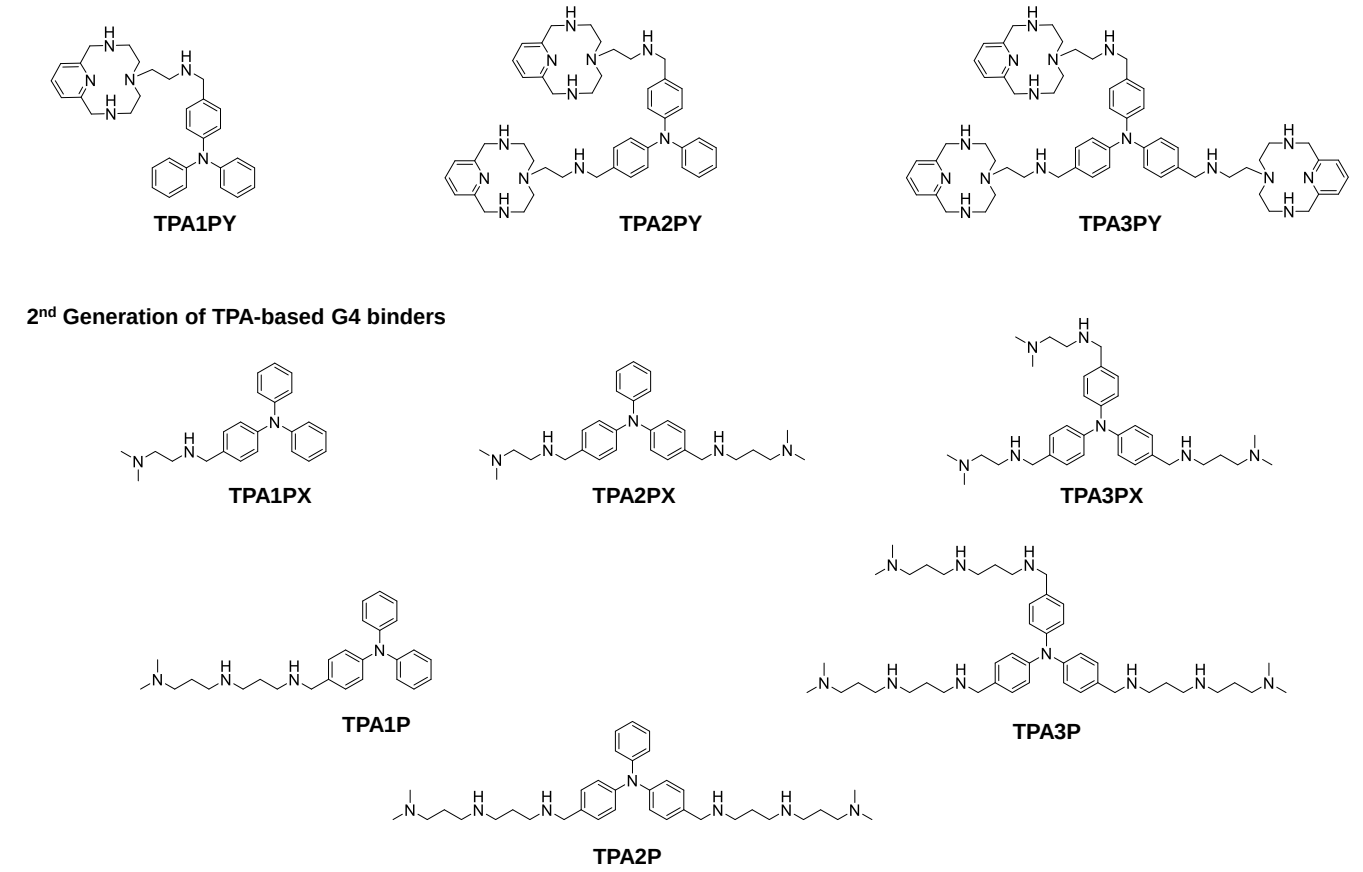

Figure 1. Triphenylamine-based derivatives corresponding to the 1st generation and 2nd generation of designed compounds.

Results and Discussion

Synthesis of TPA-based ligands

All six second-generation molecules were obtained by condensation of the corresponding triphenylamine aldehyde with one, two or three equivalents of the respective polyamine in dry ethanol (Figures S24-29). Then, the resulting imines were reduced using $NaBH_4$ and precipitated as hydrochloride salts with HCl. All the molecules were fully characterized by NMR spectroscopy (^1H and ^{13}C), mass spectrometry (HR-MS) and elemental microanalysis (see Experimental Details and ESI). The synthetic procedure is based on a one-pot protocol with simple work-up, which gives the final compounds in high yields.

Acid-base properties of the ligands

Polyamine based ligands, as those shown herein, have a wide range of protonation states as a function of pH. [12] The introduction of positive charges favours the establishment of strong electrostatic interactions and hydrogen bonding formation with anionic species, such as DNA.[13] Therefore, before proceeding to study the DNA binding of the new ligands, we assessed their acid-base behaviour by both potentiometry and spectroscopy.

Potentiometric studies were used to determine the stepwise protonation constants of the ligands (Table 1) and to calculate the distribution diagrams of species (Figures S1-S6). All the ligands showed the same number of protonation steps than their number of secondary and tertiary amine groups, excluding the amine of the triphenylamine core. The very low basicity of the

Table 1. Logarithms of the stepwise protonation constants of the TPA-based ligands obtained by potentiometric titrations.[a]

Reaction[b]	TPA1PX	TPA2PX	TPA3PX	TPA1P	TPA2P	TPA3P
H + L ⇄ HL	8.23(2)[c]	9.16(2)	9.88(1)	8.93(1)	10.27(1)	10.66(2)
H + HL ⇄ H_2L	6.28(2)	9.03(1)	9.02(1)	8.87(1)	9.42(5)	10.22(6)
H + H_2L ⇄ H_3L		6.60(2)	8.93(1)	7.33(1)	8.75(2)	9.91(2)
H + H_3L ⇄ H_4L		5.72(2)	6.86(1)		8.61(1)	9.27(1)
H + H_4L ⇄ H_5L			5.87(1)		7.49(2)	8.76(1)
H + H_5L ⇄ H_6L			5.50(1)		7.10(2)	8.37(1)
H + H_6L ⇄ H_7L						7.77(1)
H + H_7L ⇄ H_8L						7.29(1)
H + H_8L ⇄ H_9L						6.82(1)
log β[d]	14.51(2)	30.52(2)	46.07(1)	25.13(1)	51.64(2)	78.98(1)
Mean positive charge at pH = 7.4	1.0	2.1	3.2	2.4	4.8	7.3

[a] Experiments were carried out in a 0.15 M NaCl aqueous solution at 298.1±1 K. [b] Charges omitted for clarity. [c] Values in parentheses are standard deviations in the last significant figure. [d] log β=∑ log K.

triphenylamine moiety prevents the determination of a protonation constant associated to this unit. Hence, **TPA1PX** has two, **TPA1P** has three, **TPA2PX** has four, **TPA3PX** and **TPA2P** have six, and **TPA3P** shows nine protonation steps in the pH range of study (2.5 – 10.5). The average number of protons of the ligands at pH = 7.4 is shown in the last row of Table 1.

The acid-base behaviour of the ligands can be arranged in two categories, one comprises the ligands containing the shorter polyamine chains (**TPA1PX**, **TPA2PX** and **TPA3PX**) and a second group with the ligands featuring longer chains (**TPA1P**, **TPA2P** and **TPA3P**). The former group presents two sets of values of stepwise protonation constants, one of high and the other one of medium values, and these values decrease according to statistical probability and electrostatic repulsions.

For each ligand the first protonation process might occur at the tertiary amines of the linear chains and, once all of them are protonated, the following steps take place at the secondary amine groups. Regarding the second group of ligands compressing the longer branched derivatives, TPA-P, the decrease between the values of the successive stepwise constants is milder because the longer chains reduce the electrostatic repulsions and increase inductive effects facilitating protonation processes to occur. A tentative protonation pattern could be proposed taking into account the basicity of the amines and the minimisation of electrostatic repulsions. The first protonation steps might occur at the tertiary amines of the chain and then, the secondary amines more separated from these ones closer to the TPA moiety might be protonated. The secondary amines at the centre of the chain should be the last ones in bearing protonation. We conducted NMR experiments at different pD values to confirm the protonation patterns although, unfortunately, ^{1}H NMR signals become very broad upon increasing the pH indicating aggregation, which hampered the interpretation of the results.

Following the potentiometric studies, the absorption and fluorescence emission spectra of the ligands were recorded as a function of pH to get insight into the protonation dependence of these photophysical properties.

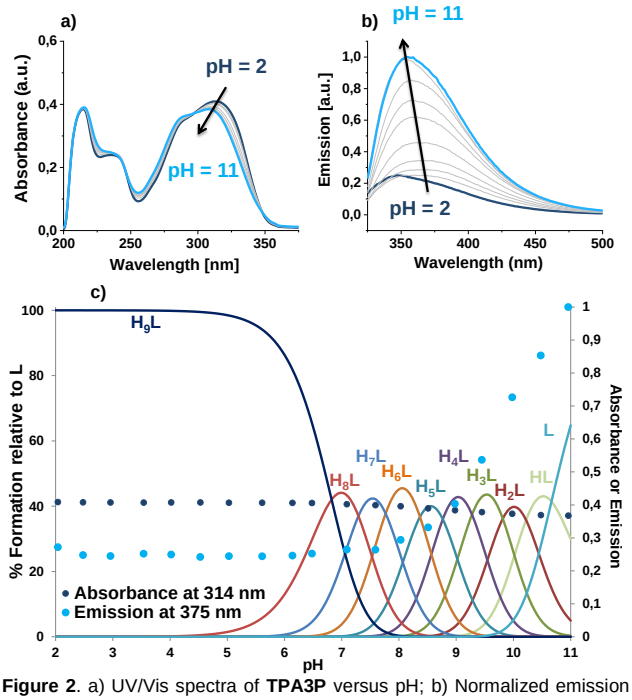

Figure 2. a) UV/Vis spectra of **TPA3P** versus pH; b) Normalized emission of **TPA3P** versus pH and c) Molar fraction distribution diagram for protonated species of **TPA3P** superposed to its normalized emission at 375 nm (λ_{ex} = 314 nm (●) and the absorbance at 314 nm (●).

The UV-Vis spectra of the ligands show a band centred at 285 – 330 nm, which is associated to the π-π* transition of the triphenylamine moiety.[14] This absorption band experiences a slight hyperchromic red shift upon decreasing the pH, which becomes larger as the number of amines increases (Figure 2 and S1-S6).

With respect to the fluorescence emission, when exciting at 314 nm, all the ligands show a large enhancement and a blue shift upon increasing the pH, which becomes more remarkable as the number of branches of the ligand increases (Figure 2 and S1-S6). These variations may be attributed to an aggregation-induced emission (AIE) effect, as we previously reported for the first-generation of ligands.[11] The high charge of the ligands at acidic pH hampers the occurrence of intermolecular interactions, which enables the relaxation of the excited state through a non-radiative pathway, resulting in a quenching of the fluorescence emission. On the other hand, the deprotonation of these ligands at high pH favours the formation of intermolecular interactions and induces aggregation, which constrains the intermolecular rotation of the TPA moiety. The restriction of this rotation causes the appearance of an AIE effect with the concomitant enhancement of the fluorescence emission.

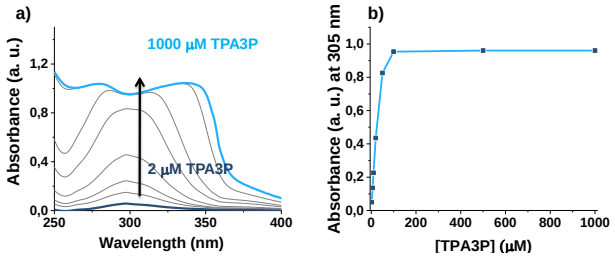

Figure 3. a) UV/Vis spectra upon increasing **TPA3P** concentration at pH 12 b) absorbance at 305 nm versus **TPA3P** concentration at pH 12.

To corroborate the formation of aggregates, UV/Vis and emission spectra of the tri-branched ligands (**TPA3PX** and **TPA3P**) with different concentrations at high pH (pH = 12) were recorded (Figures 3 and 4). The absorption profile of both ligands changes upon increasing the ligand concentration until reaching a saturation point, which confirms the formation of nanoaggregates (Figure 3 and Figure S7).[15]

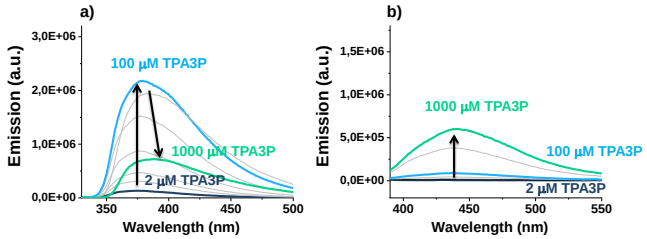

Figure 4. a) Emission spectra of increasing **TPA3P** concentrations at pH 12 (λ_{ex} = 314 nm), b) Emission spectra of increasing **TPA3P** concentrations at pH 12 (λ_{ex} = 375 nm) and c) Depiction of the aggregated state formation and the AIE effect.

Regarding the emission spectra of **TPA3PX** at increasing concentrations when irradiating at 314 nm, the excitation wavelength corresponding to the ligand, a blue-shifted enhancement is observed without the emergence of a new emission band, which is associated with a weak AIE effect (Figure S3). [16] In contrast, **TPA3P** displays a striking blue-shift and fluorescence enhancement upon increasing the ligand concentration up to 100 µM, followed by a red-shifted quenching at higher ligand concentrations (Figure 4a). Moreover, by using a longer wavelength, optimal for the excitation of the aggregates (375 nm), **TPA3P** shows no fluorescence emission in dilute solutions (< 20 µM). However, the emission experiences a 100-fold enhancement (Figure 4b) at the concentrations in which aggregates are formed, confirming the remarkable AIE effect.

Interaction with G-quadruplex DNA

FRET melting assays

An initial evaluation of the stabilisation of the DNA models induced by the ligands was conducted using FRET melting assays. A selection of the ΔT_m values of G4 DNA provided by the interaction with the TPA-PX and TPA-P ligands are plotted in Figures 6a and 6b. The remaining data are compiled in Tables S3, S4 and S5 in ESI. These data show that the stabilisation effect is more prominent as the number of branches increases. The series of TPA-P ligands showed larger G4 stabilisations than the TPA-PX series, which display ΔT_m lower than 6 ºC for all G4s used. Within each series of ligands, the higher G4 DNA stabilisation is induced by the tri-branched ligand followed by the di- and the mono-branched ones. These results reflect the importance of the number of secondary amines and their protonation state (i.e. positive charges) on the supramolecular interactions established between the ligands and the G4 DNA structures. This relationship is clearly showed by the linear relationship obtained when plotting the ΔT_m values against the average number of positives charges of the ligands at pH 7.4 calculated from the protonation constants. (Figure 5). Moreover, the same trend is observed within the first-generation ligands that we previously reported. [11]

Within the TPA-P series of ligands, telomeric G4s were more strongly stabilised than the rest of G4 DNA sequences. This was particularly notable for HTelo-21 in sodium buffer, which adopts an antiparallel G4 conformation. More interestingly, the stabilisation of duplex DNA was negligible, denoting the remarkable selectivity for G4s over duplex DNA (Figure 6).

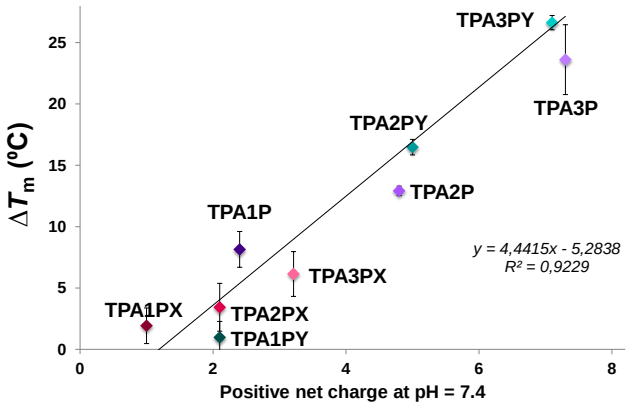

Figure 5. Plot of the ΔT_m [ºC] values for HTelo21-Na (0.2 µM) and the studied compounds (ligand-to-G4 ratio of 5) versus the positive net charge at pH = 7.4, calculated from the distribution diagrams of species.

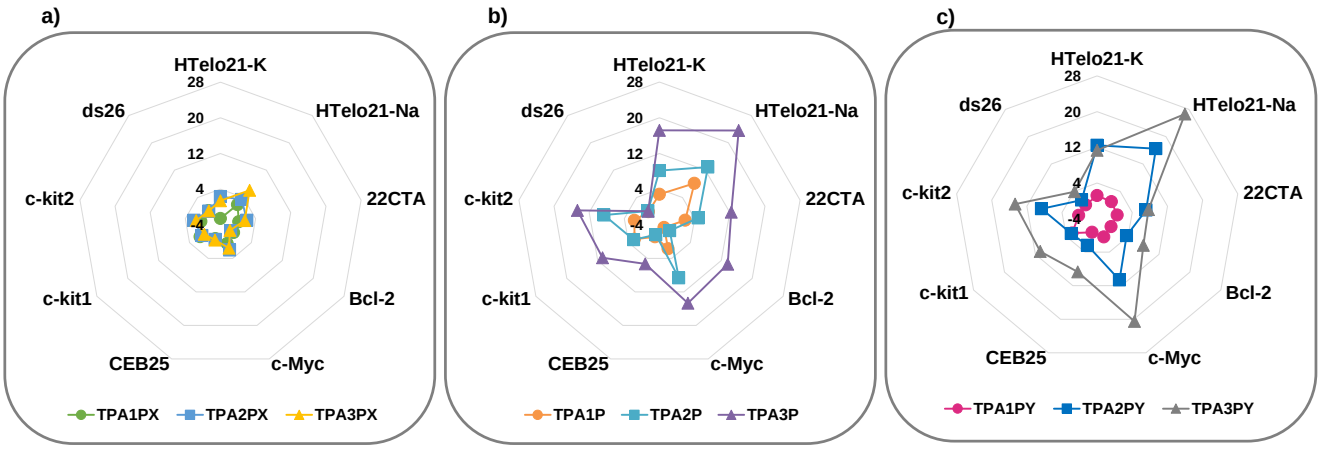

Figure 6. Radar plot of ΔT_m (ºC) for the interaction between the first- and second-generation TPA ligands and various DNA sequences. The values were determined (in triplicate) by conventional FRET melting assays using 0.2 μM of oligonucleotide and 1 μM of compounds being tested. The values of a) are taken from ref. 9.

In comparison with the first-generation of TPA-based ligands, the tri-branched **TPA3P** has generally similar stabilisation effect than the strongest stabiliser of the former series, **TPA3PY** (Figure 6b and 6c). [11] These results indicate that the G4 stabilising ability of the ligand is retained when replacing the three macrocyclic pendant arms of **TPA3PY** by the linear *N,N*-dimethyldipropylenetriamine groups in **TPA3P**. In addition, the stabilisation induced by **TPA3P** is similar to that of some well-established G4 binders such as PDS, 360A and Ni-salphen complexes. [17]

Intriguingly, the double-stranded stabilisation displayed by **TPA3P** is negligible ($\Delta T_m \approx 0$ ºC), whereas the first-generation compound, **TPA3PY**, showed a slight stabilisation effect ($\Delta T_m \approx 4$ ºC). This fact highlights the G4 selectivity improvement achieved by the introduction of flexible polyamine-based substituents in the molecular design of the TPA-based ligands.

To evaluate more thoroughly the selectivity of the ligands for G4 over duplex DNA, we performed FRET-melting competition assays, in which we added a duplex competitor. Interestingly, the addition of increasing amounts of duplex DNA does not shift significantly the high ΔT_m values of HTelo21-Na and Bcl-2 (Figure S10). At duplex-to-G4 ratio of 100 the ΔT_m only decrease 3 ºC for HTelo21-Na and Bcl-2. These results support the noteworthy **TPA3P** selectivity for G4 DNA over duplex DNA.

Fluorescence emission studies

The binding affinity was assessed by fluorescence titrations. We monitored the emission of the ligands in the presence of different DNA sequences at two different excitation wavelengths, one corresponding to the ligands, 314 nm, and the other associated with their aggregates, 375 nm (Figures 7 and S10 – S20).

The tri-branched ligand **TPA3P** displayed a decrease in the emission intensity at 384 nm with a concomitant blue shift when excited at 314 nm (Figures 7a and 7c), while interestingly, a large emission band appeared centred at 445 nm, when exciting at 375 nm (Figure 7b and 7d). Indeed, the fluorescence emission intensity shows around a 20-fold increase upon interaction with the G4 HTelo21-Na, while the duplex control yields a remarkably lower 5-fold increase (Figure 7e). Otherwise, the emission of the bi-branched and mono-branched ligands (**TPA2P** and **TPA1P**) experiences a lower intensity change than **TPA3P** (Figures S17-S20).

As already discussed for **TPA3PY**,[11] the fluorescence enhancement observed when exciting at 375 nm can be ascribed to an AIE effect produced by formation of **TPA3P**-G4 aggregates. The binding constants derived from the fluorescence titrations are shown in Table 2 and Figures S21-S23. The values of the constants associated to the tri-branched **TPA3P** ligand are from two to four orders of magnitude higher than those of the bi- and mono-branched ligands, respectively. In addition, the stability constant calculated for the interaction of the duplex DNA d26 with TPA3P ($\log K_a = 2.3(4)$) is at least three orders of magnitude lower than the values obtained for the G4s (Table 2). Consequently, the tri-branched compound displays quantitative analytical discrimination between G4 DNA and duplex DNA. These results are consistent with the FRET melting studies, highlighting the remarkable affinity and selectivity of **TPA3P** for G-quadruplex DNA structures.

In comparison to the first-generation analogue (**TPA3PY**),[11] **TPA3P** shows a significant improvement in selectivity without compromising the high affinity towards G4 DNA. Therefore, the molecular design herein presented, with flexible and adaptive polyamine substituents, leads to an effective recognition of G4 DNA.

Table 2. Logarithms of affinity constants (log K_a) calculated from the fluorimetric titrations for the system **TPA-P**-DNA.

Compound	DNA Sequence	log K_a[a]
TPA3P	HTelo22-K	6.0(1)
	HTelo22-Na	5.5(5)
	22CTA	6.1(1)
	Bcl-2	7.2(3)
	CEB25	5.8(5)
	c-Myc	5.31(2)
	c-kit1	6.5(2)
	c-kit2	7.0(4)
	ds26	2.3(4)
TPA2P	HTelo22-K	3.4(2)
	ds26	3.5(1)
TPA1P	HTelo22-K	1.6(3)
	ds26	1.3(4)
TPA3PY[11]	HTelo22-K	6.7(4)
	HTelo22-Na	6.6(6)
	22CTA	6.5(2)
	Bcl-2	7.2(1)
	CEB25	7.4(3)
	c-Myc	6.3(4)
	c-kit1	7.0(2)
	c-kit2	8.0(6)
	ds26	6.2(3)

[a] Number in parenthesis are standard deviations in the last significant figures.

Circular dichroism studies

The effect on the DNA conformation upon binding the TPA-based ligands was studied by circular dichroism spectroscopy (CD). We firstly assessed the modification of the CD spectrum corresponding to the hybrid telomeric G4 DNA, HTelo22-K (Figures 8a, 8b and 8c). In general, the addition of the ligand led to a decrease in the intensity of the bands associated to G4 DNA. Addition of **TPA1P** did not lead to any significant change in the shape of the CD spectrum. On the other hand, increasing additions of **TPA3P** did modify significantly the overall CD spectrum of HTelo22-K. These changes could be due to intense induced bands (from the ligand) rather than an overall change in G4 topology. However, the loss of ellipticity can also be due to the G4 structure unfolding. While all other data presented herein suggests that **TPA3P** is clearly a good G4 binder, the decrease in ellipticiy in the CD studies could be interpreted as changes in the DNA secondary structure (including disassembly of the G4 structure). This has also been observed for other ligands such as extended porphyrins (derivatives of TMPyP4).[18] In spite of the reduction in ellipticity of the G4 bands (at *ca*. 240, 265 and 295 nm), in all three cases new induced CD (ICD) bands centred at 230 and 330 nm emerge.

These modifications in the G4 CD spectrum are more pronounced as the number of amine groups of the compound increases (**TPA3P** > **TPA2P** > **TPA1P**), which is consistent with the higher G4 affinity found for the extensively substituted TPA compounds.

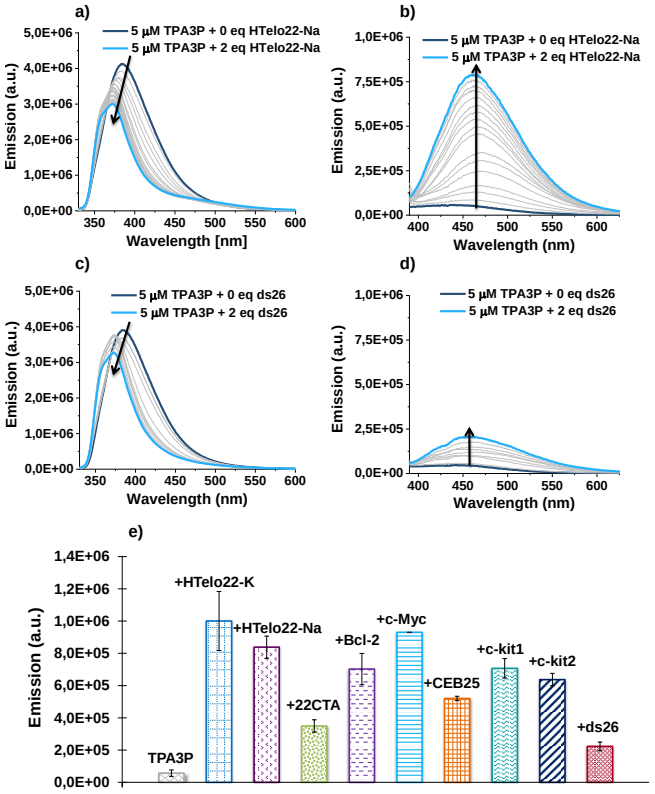

Figure 7. Fluorimetric titration of **TPA3P** with 2 equivalents of DNA (HTelo22-K, a and b; ds26, c and d) at different excitation wavelengths (a and c, λ_{ex} = 314 nm; b and d, λ_{ex} = 375 nm). e) Emission change experienced upon the addition of different DNA sequences to a solution of **TPA3P** (λ_{ex} = 375 nm).

The CD spectra of the parallel c-Myc G4 structure shows two bands, one positive centred at 265 nm and one negative centred at *ca*. 240 nm (Figure 8d, 8e and 8f). Upon addition of the TPA derivatives, a decrease in the intensity of both CD bands is observed, but the preservation of the CD spectrum features indicates that the interaction between the ligands and c-Myc does not cause the disruption of the G4 structure. However, the decrease of the intensity of the bands may suggest that the interaction with the ligands modifies the disposition of the G-tetrads.

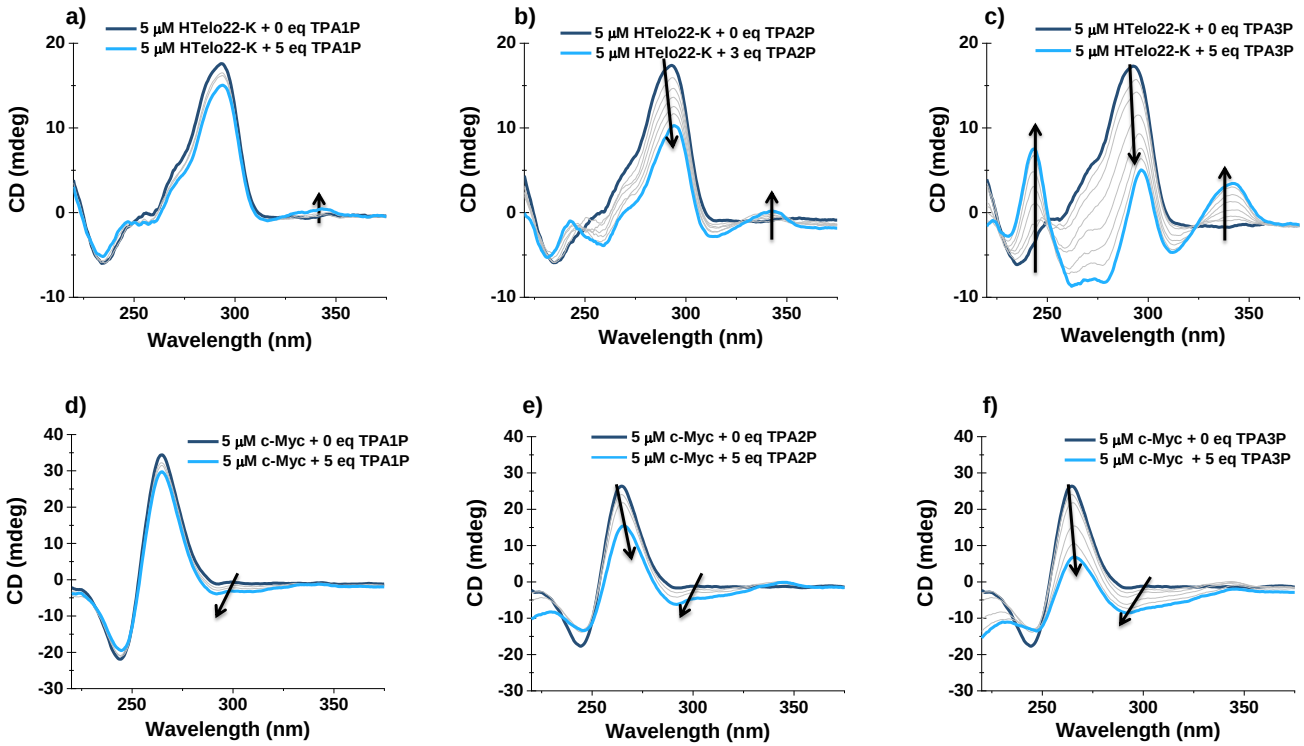

Figure 8. CD titrations of 5 μM HTelo22-K with a) **TPA1P,** b) **TPA2P** and c) **TPA3P**. CD titrations of 5 μM c-Myc with d) **TPA1P,** e) **TPA2P** and f) **TPA3P.**

Molecular Modelling

In order to get insight into the intriguing G4 DNA preference of **TPA3P** in comparison to **TPA3PY**, we conducted molecular modelling of the interaction between both compounds and G-quadruplex DNA, as well as duplex DNA. We built the model of G4 DNA from the hybrid conformation HTelo22 (PDB: 2JSK, see Materials and Methods), positioning potassium ions in the central channel. The double stranded DNA model was constructed with a B-type conformation (ds26), prevalent among genomic material. During all the calculations, the water solvent molecules were considered explicitly following the TIP3PBOX model, neutralising the system with sodium ions (see Materials and Methods).

An example of one representative minimum energy conformer for the interaction between G4 DNA and **TPA3P** is illustrated in Figure 10a and S30. The triphenylamine core is π-π stacked onto one of the G-tetrads, while the polyamine substituents are embracing the structure and exerting electrostatic interactions between the protonated ammonium groups of the ligands and the phosphate backbone of the DNA. This binding model highlights the importance of the electrostatic forces in the interaction between the G4s and the TPA derivatives: the higher the number of branches, the larger the stabilisation and affinity towards the G4 DNA. Not surprisingly, the minimum energy conformers resulting from the interaction of HTelo22 with **TPA3PY** showed a similar binding mode than **TPA3P,** in which TPA stacks onto the G-tetrad and the macrocyclic substituents interact with the DNA backbone (Figure 10b). Moreover, it is noteworthy that for both ligands the tertiary nitrogen atom of the triphenylamine core is not aligned with the ionic channel of the G-quadruplex (Figure S30).

In contrast, the molecular modelling corresponding to the interaction between the compounds and ds26 led to different results (Figure 10c and 10d). The linear polyamine substituents of **TPA3P** establish electrostatic interactions with solely one DNA strand, without significant modification of the helical structure. However, the macrocyclic substituents of **TPA3PY** interact simultaneously with the backbone of both DNA strands, which causes a structural compaction of the helix through the minor groove (elongation of the major groove of ~ 9 Å and contraction of the minor groove of ~ 5 Å).

Consequently, these results indicate that the interaction between **TPA3PY** and ds26 yields a more stable conformer than that one obtained with **TPA3P**. This might explain the lower affinity of **TPA3P** towards duplex DNA, and hence, its ability of selectively recognise G4 DNA.

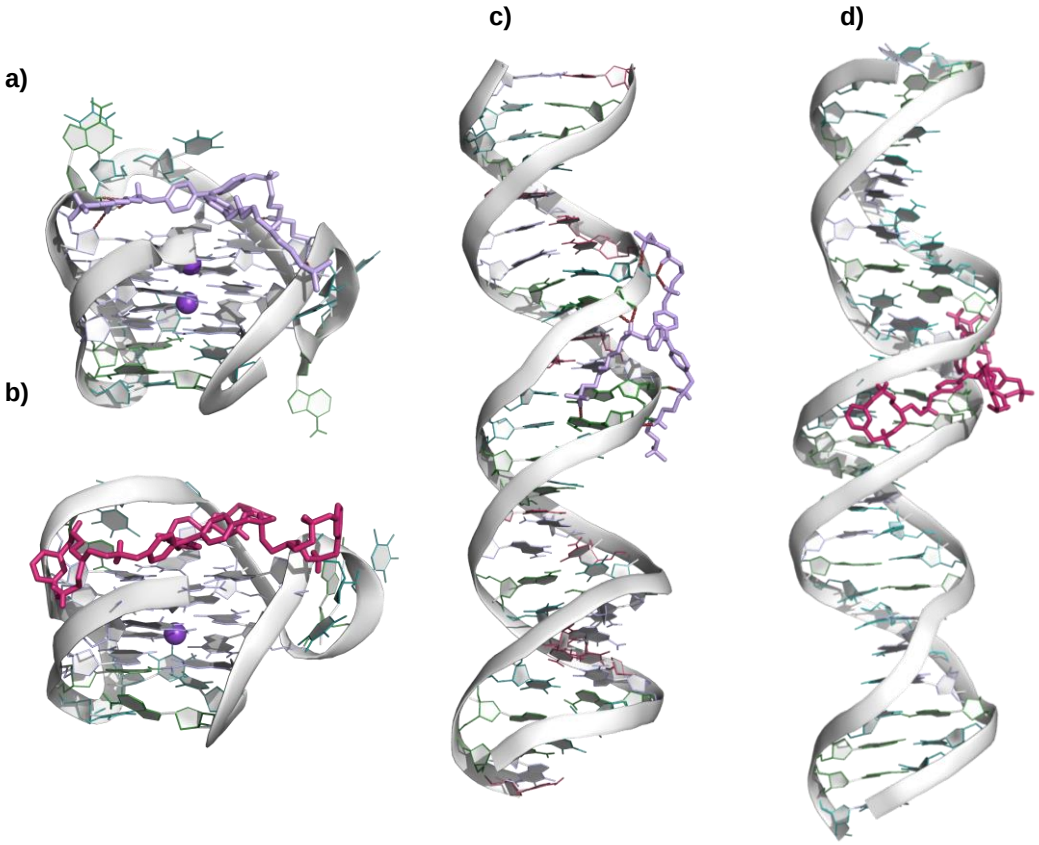

Figure 10. Models obtained by means of molecular modelling for the interaction between the G4 DNA model with **TPA3P** (a) or **TPA3PY** (b) and the interaction between the duplex model with **TPA3P** (c) or **TPA3PY** (d).

Conclusions

Six novel triphenylamine-based ligands bearing one, two or three polyamine-based substituents (**TPA1PX**, **TPA2PX**, **TPA3PX**, **TPA1P**, **TPA2P** and **TPA3P**) have been synthesised and fully characterised. The ligands behave as polyprotic bases in which the tertiary and secondary amines (except for the triphenylamine group) might be protonated depending on the pH range under study. The deprotonation of the ligands, particularly for the tri-branched **TPA3PX** and **TPA3P**, leads to an increase in the fluorescence emission ascribed to a molecular aggregation effect.

The ligands display different stabilisation effects towards G-quadruplex DNA depending on the number of amine groups. Among them, the tri-branched **TPA3P** induces the highest G4 thermal stabilisation. In addition, **TPA3P** shows a remarkable selectivity for G4s over duplex structures, as evidenced by FRET melting competition assays.

Consistent with the FRET melting experiments, **TPA3P** displays significantly higher affinity constants for G4 DNA structures than for the duplex DNA model. It is noteworthy that this selectivity is two orders of magnitude larger for **TPA3P** than for the analogous first-generation compound (**TPA3PY**).

Circular dichroism studies are less conclusive. While clear induced bands (associated to the ligand) appear in the spectra, there is an overall decrease in ellipticity for the interaction of **TPA3P** with G4 DNA.

Lastly, molecular modelling has shown a similar binding mode for both **TPA3P** and **TPA3PY** with HTelo G4: the triphenylamine moiety stacks on the top of the G-tetrad and the substituents wrap around the G4 structure displaying electrostatic and hydrogen bonding interactions. However, the ligands show a different binding mode with dsDNA. **TPA3PY** binds in the duplex minor groove and shows a large number of electrostatic contacts and hydrogen bonds between the amine groups and the phosphates in both DNA strands, causing a compaction of the groove. On the other hand, **TPA3P** solely interact with one out of the two strands, displaying a lower overall interaction with dsDNA. This fact may justify the large preference for G-quadruplex structures shown by this second-generation ligand.

Experimental Section

Materials and Methods

All reagents were obtained from commercial sources. ^{1}H NMR and ^{13}C NMR spectra were recorded on either a Bruker Advance 400 spectrometer operating at 399.96 MHz for ^{1}H and at 100.6 MHz for ^{13}C. For the ^{13}C NMR spectra, dioxane was used as a reference standard (δ 67.4 ppm), and for the ^{1}H spectra, the solvent signal was used. Mass spectrometric analysis was performed on a LCT Premier mass spectrometer.
The oligonucleotides HTelo DNA (5'-AGGGTTAGGGTTAGGGTTAGGG-3'), c-Myc (5'-TGAGGGTGGGTAGGGTGGGTAA-3'), 22CTA (5'-AGGGCTAGGGCTAGGGCTAGGG-3'), c-kit1 (5'-AGGGAGGGCGCTGGGAGGAGGG-3'), c-kit2 (5'-CGGGCGGGCGCGAGGGAGGGG-3'), CEB25 (5'-AAGGGTGGGTGTAAGTGTGGGTGGGT-3'), Bcl-2 (5'-GGGCGCGGGAGGAATTGGGCGGG-3') and ds26 (5'-CAATCGGATCGAATTCGATCC GATTG-3') were purchased from Eurogentec. The labelled oligonucleotides of the same sequence derivatized with 5'-FAM and 3'-TAMRA dyes were purchased from Eurogentec. Ligands were dissolved in milliQ water to give 2 mM stock solutions. All solutions were stored at -20 ºC and defrosted immediately before use using a suitable buffer to yield the appropriate concentrations.

General procedure for the synthesis

A solution of the corresponding mono-, bi-, or tri-aldehyde of the triphenyamine (1 – 2 mmol) dissolved in 150 mL of anhydrous ethanol was added dropwise to a solution of 1, 2 or 3 equivalents of the polyamine substituent dissolved in 50 ml of dry ethanol. The mixture was stirred under nitrogen for 12 hours at room temperature resulting in the formation of the Schiff base. The reduction of the imines was carried out by adding 10 equivalents of $NaBH_4$ and further stirring during 2 hours. Then, the solvent was removed under reduced pressure. The resulting residue was treated with H_2O (20 mL) and extracted with CH_2Cl_2 (3 x 30 mL). The organic phase was dried over Na_2SO_4 and evaporated to afford a yellow oil, which was dissolved with anhydrous ethanol and precipitated with HCl in dioxane (0.4M), yielding to the hydrochloride salt of the product.

4-[5-methyl-(2,5-diazahex-1-yl)]triphenylamine (**TPA1PX**). Yield: 50 %. ^{1}H NMR (300 MHz, D_2O): δ = 7.22 (d, *J* = 6 Hz, 2H), 6.92 – 6.88 (m, 4H), 6.78 – 6.72 (m, 8H), 4.14 (s, 2H), 3.64 – 3.52 (m, 4H), 3.00 (s, 6H). ^{13}C NMR (75.2 MHz, D_2O): δ = 151.56, 149.51, 133.84, 132.19, 127.20, 125.89, 125.24, 55.07, 53.78, 46.09, 43.72. ESI-MS m/z (%): 346.1 ($[M+H]^+$). Elemental analysis calcd (%) for $C_{23}H_{27}N_3 \cdot$ 2HCl (418.41 g/mol): C 66.0; H 6.9; N 10.0; found: C 65.4; H 6.5; N 9.8.

4,4'-bis[5-methyl-(2,5-diazahex-1-yl)]triphenylamine (**TPA2PX**). Yield: 58 %. ^{1}H NMR (300 MHz, D_2O): *δ* = 7.44 – 7.36 (m, 6H), 7.24 – 7.10 (m, 7H), 4.31 (s, 4H), 3.60 (s, 8H), 3.02 (s, 12H). ^{13}C NMR (75.2 MHz, D_2O): *δ* = 149.25, 147.22, 131.90, 130.57, 125.23, 124.92, 124.54, 124.14, 52.84, 51.91, 43.79, 41.16. ESI-MS: *m/z* 446.3 ($[M+H]^+$). Elemental Analysis calcd (%) for $C_{28}H_{39}N_5 \cdot 4HCl \cdot 1H_2O$ (609.12 g/mol): C 55.2; H 7.4; N 11.5; found: C 55.4; H 7.9; N 11.3.

4,4',4''-tris[5-methyl-(2,5-diazahex-1-yl)]triphenylamine (**TPA3PX**) Yield: 62 %. ^{1}H NMR (300 MHz, D_2O): *δ* = 7.48 – 7.45 (m, 6H), 7.26 – 7.23 (m, 6H), 4.34 (s, 6H), 3.62 (s, 12H), 3.03 (s, 18H). ^{13}C NMR (75.2 MHz, D_2O): *δ* = 148.62, 131.73, 125.31, 125.06, 52.83, 51.64, 43.81, 41.44. ESI-MS: *m/z* 546.4 ($[M+H]^+$). Elemental Analysis Calcd (%) for $C_{35}H_{51}N_7 \cdot 6HCl \cdot 2H_2O$ (800.12 g/mol): C 50.0; H 7.5; N 11.9; found: C 49.1; H 8.0; N 11.7.

4-[10-methyl-(2,6,10-undecaphan-1-yl)]triphenylamine (**TPA1P**) Yield: 53 %. ^{1}H NMR (300 MHz, D_2O): *δ* = 7.24 (d, *J* = 9 Hz, 2H), 7.05 – 7.00 (m, 4H), 6.89 – 6.84 (m, 8H), 4.09 (s, 2H), 3.32 – 3.27 (m, 2H), 3.22 – 3.14 (m, 6H), 2.95 (s, 6H), 2.26 – 2.14 (m, 4H). ^{13}C NMR (75.2 MHz, D_2O): δ = 149.09, 147.43, 131.52, 129.92, 125.10, 124.00, 123.07, 54.61, 51.15, 45.11, 44.90, 44.19, 43.24, 23.12, 21.65. ESI-MS: *m/z* 417.0 ($[M+H]^+$). Elemental Analysis Calcd (%) for $C_{27}H_{36}N_4 \cdot 3HCl \cdot 1H_2O$ (543.99 g/mol): C 59.6; H 7.6; N 10.3; found: C 60.2; H 8.3; N 11.7.

4,4'-bis[10-methyl-(2,6,10-undecaphan-1-yl)]triphenylamine (**TPA2P**) Yield: 61 %. ^{1}H NMR (300 MHz, D_2O): *δ* = 7.43 – 7.37 (m, 6H), 7.24 – 7.16 (m, 7H), 4.24 (s, 4H), 3.33 – 3.18 (m, 16H), 2.95 (s, 12H), 2.26 – 2.13 (m, 8H). ^{13}C NMR (75.2 MHz, D_2O): *δ* = 148.87, 147.20, 131.57, 130.23, 125.95, 124.91, 124.12, 54.61, 51.14, 45.08, 44.86, 44.11, 43.23, 23.05, 21.62. ESI-MS: m/z 588.3 ($[M+H]^+$). Elemental Analysis Calcd (%) for $C_{36}H_{57}N_7 \cdot 6HCl$ (806.23 g/mol): C 50.8; H 13.9; N 11.2; found: C 53.6; H 7.9; N 12.1.

4,4',4''-tris[10-methyl-(2,6,10-undecaphan-1-yl)]triphenylamine (**TPA3P**) Yield: 72 %. ^{1}H NMR (300 MHz, D_2O): *δ* = 7.45 (d, *J* = 10 Hz, 6H), 7.24 (d, *J* = 9 Hz, 6H), 4.27 (s, 6H), 3.33 – 3.20 (m, 24H), 2.95 (s, 18H), 2.28 – 2.13 (m, 12H). ^{13}C NMR (75.2 MHz, D_2O): *δ* = 148.50, 131.65, 125.70, 124.96, 54.61, 51.16, 45.09, 44.87, 44.23, 43.23, 23.06, 21.63. ESI-MS: *m/z* 759.53 ($[M+H]^+$). Elemental Analysis Calcd (%) for $C_{45}H_{78}N_{10} \cdot 9HCl \cdot 8H_2O$ (1231.33 g/mol): C 43.9; H 8.4; N 11.4; found: C 45.7; H 10.9; N 11.6.

EMF measurements

The potentiometric titrations were carried out at 298.1 ± 0.1 K using NaCl 0.15 M as supporting electrolyte. The experimental procedure (burette, potentiometer, cell, stirrer, microcomputer etc.) has been fully described elsewhere. [19] The acquisition of the data was performed with the computer program PASAT. [19] The reference electrode was an Ag/AgCl electrode in saturated KCl solution. The glass electrode was calibrated as a hydrogen ion concentration probe by titration of previously standardized amounts of HCl with CO_2-free NaOH solutions and the equivalent point determined by the Gran's method, which gives the standard potential, E_0', and the ionic product of water (pK_w = 13.73(1)). The computer program HYPERQUAD was used to calculate the protonation and stability constants. [19] At least two measurements were performed for each system. The HYSS program was used to obtain the distribution diagrams. [19]

FRET melting assay

Labelled DNA was dissolved as a 20 μM stock solution in MilliQ water, then they were annealed as a 400 nM concentration in potassium/sodium cacodylate buffer (pH 7.3), depending on the G4, at 95 ºC for 5 min. Finally, the solutions were allowed to cool slowly to room temperature overnight. The buffer used for the antiparallel G4 HTelo- Na was 10 mM NaCl, 90 mM LiCl, 10 mM LiCac, for the G4 c-Myc was 1 mM KCl, 99 mM LiCl, 10 mM LiCac and for the rest of DNA was 10 mM KCl, 90 mM LiCl, 10 mM LiCac). Ligands were dissolved from stock solutions (see above) to the appropriate final concentrations in the buffer. Each well of a 96- well plate (Applied Biosystem) was prepared with 60 μL, with a final 200 nM DNA concentration and increasing concentration of tested ligands (0–4 μM). Measurements were performed on a PCR Stratagene Mx3005P (Agilent Technologies) with excitation at 450–495 nm and detection at 515–545 nm. Readings were taken from 25 ºC to 95 ºC at interval of 0.5 ºC maintaining a constant temperature for 30 seconds before each reading. Each measurement was done in triplicate. The normalized fluorescence signal was plotted against the compound concentration and the ΔT_m values were determined.

FRET competition assay

Labelled oligonucleotides were annealed as a 400 nM concentration in potassium cacodylate buffer (10 mM KCl, 90 mM LiCl, 10 mM LiCac pH 7.3 for 22AG, 22CTA and Bcl-2; 10 mM NaCl, 90 mM LiCl, 10 mM LiCac pH 7.3 for antiparallel 22AG) at 95 ºC for 5 min, and allowed to cool slowly to room temperature overnight. Ligands were dissolved from stock solutions to final concentrations in the buffer. Each well of a 96- well plate (MJ Research, Waltham, MA) was prepared with a final 200 nM oligo concentration, 1 μM ligand concentration, and the ds26 concentration to test (0 to 500 μM). Measurements were performed under the same conditions as the FRET melting assay.

Fluorescence titrations

The DNA was dissolved in potassium cacodylate buffer (100 mM KCl, 10 mM LiCac pH 7.3) and annealed at 95 ºC for 5 min, before cooling to room temperature overnight. The concentration of DNA was checked using the molar extinction coefficients. Annealing concentrations were approximately 1 mM. For the fluorescence emission titrations, ligands (10 μM) in the same buffer were titrated with the corresponding DNA until saturation of fluorescence. The emission spectra were recorded in 1 cm path-length quartz cuvettes. The equipment used was a Varian Cary Eclipse Spectrometer. Spectra were smoothed using the Savitzky–Golay algorithm and emission maxima were fitted to 1:1 binding model using the Levenberg–Marquardt algorithm and equations previously reported. [20]

CD spectroscopy

The oligonucleotides were dissolved in Milli Q water to yield a 1 mM stock solution. They were then diluted using 10 mM Tris-HCl and 50 mM KCl (pH 7.0) buffer to 5 μM. Prior to use in the CD assay, the DNA solution was annealed by heating the solution to 95 °C for 10 min and then cooling to room temperature overnight. The CD spectra were measured in a 10 mm×2 mm rectangular cell path length cuvette. The CD spectra of the DNA

upon increasing concentrations of the ligands were measured in the spectral range of 200-600 nm.

Computational method

Molecular dynamics (MD) studies have been started with the building of the **TPA-3P** and **TPA3PY** ligands, using the basic structure reported by Hariharan *et al.* [21] (CCDC code: 1448378) for the TPA moiety, and completing the ligand structures with the help of *xleap* software. The protonation degree of **TPA3P** and **TPA3PY** was approximated to 7 in both cases taking into account the calculated protonation constants.
With regard to the DNA models, they were generated using different approaches. The ds26 system was built by using the NAB molecular manipulation language included in AMBER16[22] (Assisted Model Building with Energy Refinement) software. On the other hand, the representative HTelo22 G4 model was taken from the Protein Data Bank (PDB, ID 2JSM) [23] as a starting structure, filling it with three potassium cations. Once the DNA systems were generated, the ligands were approximated using the LEaP software and, finally, the resulting systems were solvated with the addition of 21098 water residues for the ds26/ligand system (13700 for the G-quadruplex/ligand system) using TIP3PBOX and then neutralized. [24]

Once the systems were built, they were energetically minimized and a total of 6 ns MD was performed, after an equilibration stage at 300 K. All the studies have been done using AMBER16[22] software. The organic compounds have been modelled using the *gaff*[25] force field while the *ff14SB*[26] one was used for the nuclear bases. In the same way, the environment conditions have been simulated by using the *ionsjc_tip3p* field. [24] Finally, a series of 10 minimum energy conformers were selected and then energetically optimised again. The MD simulation trajectory was analysed using the cpptraj module[27] within AmberTools17. PyMOL[28] was employed for visual inspection and to create the molecular graphics.

Acknowledgements

Financial support by the Generalitat Valenciana, Spanish MINECO and FEDER funds from the European Union are gratefully acknowledged (Project CTQ2016-78499-C6-1-R, CTQ2017-90852-REDC, Unidad de Excelencia María de Maeztu MDM-15-0538 and PROMETEO II 2015-002). I. P. appreciates her PhD grant “Atracció al Talent” given by the University of Valencia. A. M.-C. and C. G.-R. would like to thank the Spanish Ministry of Science, Research and Universities for their FPU PhD grants (FPU14/05098). J. G.-G. is much indebted to the Generalitat Valenciana for his CIDEGENT project (CIDEGENT/2018/015) and the Royal Society (NF140726, AL\170036 and AL\180021). We also acknowledge Mass Spectrometry and NMR service from the Central Services for Experimental Research (SCSIE) of University of Valencia.

Keywords: polyamine-based ligand • G-quadruplex DNA • G4 selectivity

[1] O. Ursu, M. Glick, T. Oprea, *Nat. Rev. Drug Discov.* **2019**, *18*, 328.

[2] a) S. Neidle, *Nat. Rev. Chem.* **2017**, *1*, 0041; b) S. Neidle, *J. Med. Chem.* **2016**, *59*, 5987–6011.

[3] Quadruplex Nucleic Acids, (Eds.: S. Neidle, S. Balasubramanian), RSC Publishing, Cambridge, **2006**.

[4] a) V. S. Chambers, G. Marsico, J. M. Boutell, M. Di Antonio, G. P. Smith, S. Balasubramanian, *Nat Biotechnol.* **2015**, 33, 877–881; b) A. Bedrat, L. Lacroix, J.-L. Mergny, *Nucleic Acid. Res.* **2016**, 44, 1746–1759.

[5] S. Balasubramanian, L. H. Hurley, S. Neidle, *Nat. Rev. Drug. Discov.* **2011**, *10*, 261-275.

[6] a) G. W. Collie, G. N. Parkinson, *Chem. Soc. Rev.* **2011**, *40*, 5867–5892; b) R. Simone, P. Fratta, S. Neidle, G. N. Parkinson, A. M. Isaacs, *FEBS Lett.* **2015**, *589*, 1653–1668.

[7] a) A. R. Duarte, E. Cadoni, A. S. Ressurreiçao, R. Moreira, A. Paulo, *Chem. Med. Chem.* **2018**, *13*, 869–893; b) D. Monchaud, M.-P. Teulade-Fichou, *Org. Biomol. Chem.* **2008**, *6*, 627-636; c) S. N. Georgiades, N. H. Abd Karim, K. Suntharalingam, R. Vilar, *Angew. Chem. Int. Ed.* **2010**, *49*, 4020-4034.

[8] a) J. Carvalho, T. Quintela, N. M. Gueddouda, A. Bourdoncle, J.- L- Mergny, G. F. Salgado, J. A. Queiroz, C. Cruz, *Org. Biomol. Chem*. **2018**, *16*, 2776-2786; b) J. Ferreira, T. Santos, P. Pereira, M. C. Corvo, J. A. Queiroz, F. Sousa, C. Cruz, Analyst **2017**, *142*, 2982-2994; c) R. Rodriguez, G. D. Pantos, D. P. N. Gonçalves, J. K. M. Sanders, S. Balasubramanian, Angew. Chem. Int. Ed. **2007**, *46*, 5405-5407.

[9] a) M.- Q. Wang, Z.- Y. Wang, Y.- F- Yang, G.- Y. Ren, X.- N. Liu, S. Li, J.-W. Wei, L. Zhang, *Tetrahedron Lett*. **2017**, *58*, 3296-3300; b) M.- Q. Wang, L.-X. Gao, Y.- F- Yang, X.- N. Xiong, Z.- Y. Zheng, S. Li, Y. Wu, L.- L. Ma, *Tetrahedron Lett*. **2016**, *57*, 5042-5046; c) H. Lai, Y. Xiao, S. Yan, F. Tian, C. Zhong, Y. Liu, X. Weng, X. Zhou, *Analys*t **2014**, *139*, 1834-1838.

[10] a) F. Hammerer, F. Poyer, L. Fourmois, S. Chen, G. Garcia, M.- P. Teulade-Fichou, P. Maillard, F. Mahuteau-Betzer, *Bioorg. Med. Chem.* **2018**, *26*, 107-118; b) G. Bordeau, R. Lartia, G. Metge, C. Fiorini-Debuisschert, F. Charra, M.- P. Teulade-Fichou, *J. Am. Chem. Soc*. **2008**, *130*, 16836-16837.

[11] I. Pont, J. González-García, M. Inclán, M. Reynolds, E. Delgado-Pinar, M. T. Albelda, R. Vilar, E. García-España, *Chem. Eur. J.* **2018**, *24*, 10850–10858.

[12] a) J. González-García, S. Tomic, A. Lopera, L. Guijarro, I. Piantanida, E. García-España, *Org. Biomol. Chem.* **2015**, *13*, 1732-1740; b) S. Gago, J. Gonzalez, S. Blasco, J. A. Parola, M. T. Albelda, E. García-España, F. Pina, *Dalton Trans.* **2014**, *43*, 2437-2447; c) A. Sornosa-Ten, M. T. Albelda, J. C. Frias, E. García-España, J. M. Llinares, A. Budimir, I. Piantanida, *Org. Biomol. Chem.* **2010**, *8*, 2567-2574.

[13] a) E. García-España, P. Diaz, J. M. Llinares, A. Bianchi, Coord. Chem. Rev. **2006**, *250*, 2952-2986; b) E. García-España, R. Belda, J. González, J. Pitarch, A. Bianchi in *Supramolecular Chemistry: From Molecules to Nanomaterials* (Eds.: J. W. Steed, P. A. Gale), Wiley-VCH, **2012**, pp. 1225-1257.

[14] a) M. Aydemir, G. Haykir, F. Türksoy, S. Gümüş, F. B. Dias, A. P. Monkman, *Phys. Chem. Chem. Phys.* **2015**, *17*, 25572–25582; b) B. Xu, J. He, Y. Liu, B. Xu, Q. Zhu, M. Xie, Z. Zheng, Z. Chi, W. Tian, C. Jin, F. Zhao, Y. Zhang, J. Xu, *J. Mater. Chem. C* **2014**, *2*, 3416–3428.

[15] a) B. Z. Tang, Y. Geng, J. W. Y. Lam, B. Li, X. Jing, X. Wang, A. B. Pakhomov, X. X. Zhang, *Chem. Mater.* **1999**, *11*, 1581–1589; b) Y. Hong, J. W. Y. Lam, B. Z. Tang, *Chem. Commun.* **2009**, 4332–4353.

[16] S. Y. Kim, Y. J. Cho, G. F. Jin, W. S. Han, H. J. Son, D. W. Cho, S. O. Kang, *Phys. Chem. Chem. Phys.* **2015**, *17*, 15679–15682.

[17] a) R. Rodriguez, S. Müller, J. A. Yeoman, C. Trentesaux, J.-F. Riou, S. Balasubramanian, *J. Am. Chem. Soc.* **2008**, *130*, 15758–15759; b) J. E. Reed, A. Arola, S. Neidle, R. Vilar, *J. Am. Chem. Soc.* **2006**, *128*, 5992-5993.

[18] J. Rubio-Magnieto, F, Di Meo, M. Lo, C. Delcourt, S. Clément, P. Norman, S. Richeter, M. Linares, M. Surin, *Org. Biomol. Chem*., **2015**, *13*, 2453-2463.

[19] a) L. Alderighi, P. Gans, A. Ienco, D. Peters, A. Sabatini, A. Vacca, *Coord. Chem. Rev.* **1999**, *184*, 311–318; b) A. Sabatini, A. Vacca, P. Gans, *Coord. Chem. Rev.*, **1992**, 120, 389–405; c) P. Gans, A. Sabatini, A. Vacca, *Talanta* **1996**, *43*, 1739–1753; d) H. Rossotti, F. J. C. Rossotti, *J. Chem. Educ.* **1965**, *42*, 375–378; e) G. Gran, *Acta Chem. Scand.* **1950**, *4*, 559–577; f) E. García-España, M. Ballester, F. Lloret, J. M. Moratal, J. Faus, A. Bianchi, *J. Chem. Soc. Dalton Trans.* **1988**, 101–104.

[20] a) F. H. Stootman, D. M. Fisher, A. Rodger, J. R. Aldrich-Wright, *Analyst* **2006**, *131*, 1145; b) P. Thordarson, *Chem. Soc. Rev.* **2011**, *40*, 1305–1323.

[21] P. S. Hariharan, V. K. Prasad, S. Nandi, A. Anoop, D. Moon, S. P. Anthony, *Cryst. Growth Des.* **2017**, *17*, 146–155.

[22] D.A. Case, R.M. Betz, D.S. Cerutti, T.E. Cheatham, III, T.A. Darden, R.E. Duke, T.J. Giese, H. Gohlke, A.W. Goetz, N. Homeyer, S. Izadi, P. Janowski, J. Kaus, A. Kovalenko, T.S. Lee, S. LeGrand, P. Li, C. Lin, T. Luchko, R. Luo, B. Madej, D. Mermelstein, K.M. Merz, G. Monard, H. Nguyen, H.T. Nguyen, I. Omelyan, A. Onufriev, D.R. Roe, A. Roitberg, C. Sagui, C.L. Simmerling, W.M. Botello-Smith, J. Swails, R.C. Walker,

J. Wang, R.M. Wolf, X. Wu, L. Xiao and P.A. Kollman, AMBER 2016, **2016**, University of California, San Francisco.

[23] A. T. Phan, V. Kuryavyi, K. N. Luu, D. J. Patel, *Nucleic Acids Res.* **2007**, *35*, 6517–6525.

[24] W. L. Jorgensen, J. Chandrasekhar, J. D. Madura, R. W. Impey, M. L. Klein, *J. Chem. Phys.* **1983**, *79*, 926-935.

[25] J. Wang, R. M. Wolf, J. W. Caldwell, P. A. Kollman, D. A. Case*, J. Comput. Chem.* **2004**, *25*, 1157–1174.

[26] J. A. Maier, C. Martinez, K. Kasavajhala, L. Wickstrom, K. E. Hauser, C. Simmerling, *J. Chem. Theory Comput.* **2015**, *11*, 3696–3713.

[27] D. R. Roe, T. E. Cheatham III, *J Chem. Theory Comput.* **2013**, *9*, 3084–3095.

[28] *The PyMOL Molecular Graphics System,* Version 2.0 Schrödinger*, LLC,* **2015**.

.